Measurement of electron backscattering from plastic scintillator for neutron β decay

Michael J. Betancourt

Kellogg Radiation Laboratory, California Institute of Technology, Pasadena, CA 91125, USA

An accurate measurement of the asymmetry in neutron beta decay is critical to testing the unitarity of the CKM matrix, and the possible unveiling of new physics beyond the standard model. UCN-A, an experiment currently in development at the Los Alamos National Laboratory, will study this asymmetry through the decay of polarized ultra cold neutrons. Plastic scintillators will count the beta electrons produced in the decay to obtain a measure of the asymmetry. These electrons, however, may backscatter off the scintillator necessitating a systematic correction. A clear understanding of backscattering effects is essential to an accurate correction of the data. Studies of backscattering of electrons from a scintillator target placed in a scattering chamber were performed. An electron gun produced the incident electron beam of maximum energy 120 keV. Backscattering data was obtained as a function of beam energy and intensity, with careful accounting for secondary electrons. Data were analyzed as a function of the energy and angle of the backscattered electrons with careful attention to s systematic uncertainties.

The accurate measurement of electrons produced in nuclear reactions is critical to experimental nuclear physics. Detection of electrons is often accomplished through the use of organic scintillator, a material that emits light when struck by incident electrons. Once emitted, the light is collected by a phototube where the photons are converted into an electrical charge proportional to the electron's energy. These signals are digitized and recorded by a computer producing an energy spectrum of the electrons.

Unfortunately, this process is not always perfect. Incident electrons often penetrate into the material to only a shallow depth before deflecting back towards the source. Scattered out of the scintillator, the electrons do not deposit their full energy into the scintillation, shifting the true spetrum. This phenomenon, known as electron backscattering, must be well understood for precise spectroscopy of any electron source.

At lower energies precise measurements are required for electron microscopy. Consequently, many studies of electron backscattering have been done low energies (E <40 keV) [1-3]. Moreover, sophisticated simulations that are able to model this effect exist at higher energies (E >1000 keV) [4]. In the intermediate range, however, few studies of backscattering have been done and little is known about the accuracy of the existing simulations. Hence further study into backscattering at these energies is critical to such applications as neutron β decay whose energies peak at E=782 keV.

UCN-A, an upcoming experiment, will make a precise measurement of the asymmetry in polarized neutron β decay using two symmetric plastic scintillators [5]. Ultra cold neutrons, whose energies are typically on the order of 8 m/s, will be polarized, with the two scintillators placed along the line of polarization. The neutrons then decay, emitted electrons along the line of polarization that are detected in the scintillators. Because of the precision required in the two measurements, the effects of the backscattering will have to be understood to the 20% level so that the data may be properly corrected.

Detailed studies were performed of the angular distribution of backscattered electrons, as well as the dependence of backscattering on the energy of the incident electrons.

Experimental Overview

The experiment consisted of two modes of operation: current integration mode and silicon detector mode. A beam of electrons struck a small plastic scintillator target that was housed in an iron backscattering chamber. In the current integration mode the electrons that backscattered off of the target were collected on the chamber and the resultant current was measured with precise picoammeters. The silicon detector mode featured a small silicon detector that rotated around the target, measuring how the backscattering varied around the target.

Kellogg Electron Gun

The incident beam of electrons was produced by

the Kellogg electron gun, shown in Fig 1. A hot filament emits free electrons that are extracted with a potential on the order of 6 kV. Once the electrons reach the beam line they are focused by an Einzel lens before being accelerated through a series of conducting disks held at a high potential known as the acceleration column. This potential typically ranged from 40 kV to 120 kV, producing an electron beam at energies between 34 keV and 114 keV (the accelerator potential less the extractor potential).

Steering was controlled by two perpendicular aircore coils that produced magnetic fields, allowing for horizontal and vertical control of the beam.

By varying the current in the filament, the intensity of the beam could be varied from a few electrons a second to currents as high as a few microampheres. The beam currents were typically kept at or below the nA level in order to avoid damaging the scintillator target or the silicon detector. In the current integration mode the beam currents was on the order of one nA, while the silicon detector mode featured a much smaller beam current of about 20 pA.

Previous studies of the electron gun have found that the energy of the electron beam is stable, reproducible, and monochromatic to the 0.3% level [6].

The high vacuum necessary to produce the beam was created and maintained by a system of vacuum pumps. Once a mechanical pump removed most of the atmosphere, a turbo pump achieve a typical operating pressure of 10^{-6}.

Backscattering Chamber, Targets, and Detectors

The steel backscattering chamber was placed at the end of the Kellogg electron gun to receive the beam. At the center of the chamber the plastic scintillator target was held in place with a slotted, nonconducting plastic rod. This rod could be rotated to adjust the angle of the incident beam on the target to compensate for any misalignment of the beam. In order to prevent the rod from collecting charge, a cylindrical steel sheath was placed over the rod (Fig 2). The chamber, target, and duckbill were electronically isolated from each other as well as ground so that precise current measurements could be made.

The targets themselves were comprised of organic polyvinyltoluene scintillator cut into a thin rectangular prism. Receiving the beam, the main face of prism measured 28.38 mm by 23.56 mm while the thickness was only 3.52 mm. Additionally, a small tab protruded from the top of each target. The tab slid into the target rod and, with the help of two set screws, held the target in place.

In previous studies, data were taken with an older sample of plastic scintillator. Large systematic uncertainties in the data were thought to come from crazing of the scintillator and charging. Crazing occurs when oil and other contaminates create small fractures on the surface of the scintillator over time, producing an uneven surface for the incident beam. Charging is an inherent problem with the plastic. Since polyvinyltoluene is an insulator, electrons may deposit charge within the target. The charge accumulates and deflects the incident beam.

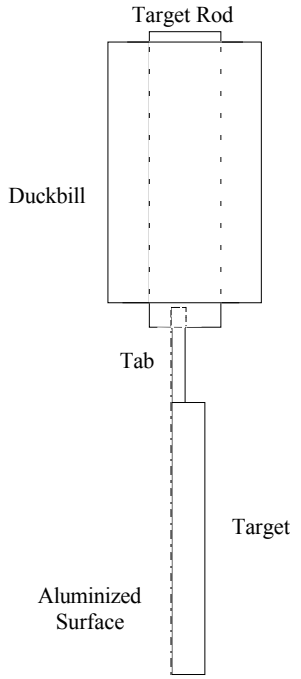

Figure 2: Schematic of the target and its support structure.

To compensate for the crazing that comes with age, unused targets were used. The targets were machines out of a large virgin piece of Eljen EJ204 plastic scintillator. Each target was carefully handled to prevent any contamination that might lead to crazing. Charging effects were neutralized with a thin layer of evaporated aluminum deposited on the surface of the scintillator. The 500 Å surface was too thin to have any effect on the backscattering. This conducting layer gave a path for any deposited charge to flow before it could accumulate and alter the incident beam.

In the current integration mode, currents from the chamber components were measured with two Kiethley 485 Autoranging Picoammeters as well as a custom built picoammeter. Those in the silicon

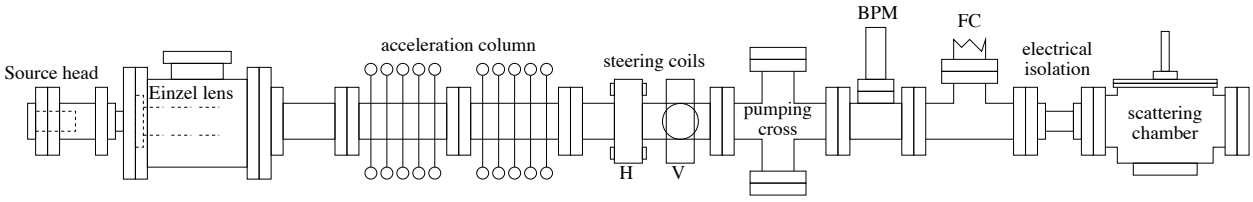

Figure 1: Diagram of the Kellogg electron gun. H and V indicate the horizontal and vertical steering coils, respectively.

detector mode were measured with an Ortec Model 439 Current Digitizer. Each detector was calibrated against each other, and all were found to agree to the picoampere level.

The silicon detector used was an Ortec model BU-13-25-3000, featuring a 25 mm^2 nominal active area and 300 μm nominal depletion depth at 100 V bias. Mounted on a rotating arm, the detector could be moved to any arbitrary angle around the target via a series of gears that were controlled by a dial on the lid of the chamber. For calibration, the detector was rotated into the incident beam. Calibration points were taken at 43.5, 63.9, 83.8, 104, and 124 keV. The calibration also gave the energy resolution of the detector, which was found to be 4.26 keV, independent of energy to less than .05 keV.

The settings of the electron gun, or tunes, were varied in order to center the beam and maximize the incident beam current. These settings included currents in the steering coils, extractor voltage, and focusing voltage. Because the scintillator illuminates when struck with a beam of significant current, the centering was done visually using a CCD camera and a small television set. The camera was placed against a window behind the target where the beam spot could be seen. Each setting was modified until a solid beam spot was centered on the scintillator.

Backscattering Measurements

For the backscattering measurements, the incident electron beam struck the target normal to its aluminized surface. Current integration data was taken for incident electron energies of 43.5, 63.9, 83.8, 104, and 124 keV, while measurements in the silicon detector mode were taken for only 124 keV

Current Integration Mode

The current integration studies measured the backscattered electrons by the current they produced on the backscattering chamber itself. Picoammeters measured the currents on the target (I_{target}) and the backscattering chamber ($I_{chamber}$). The duckbill, placed over the target rod to prevent charging, also collected a significant number of electrons scattered from the target, so this current (I_{duck}) was also taken. With these measurements, the normal incident backscattering fraction η was calculated by

$$\eta = \frac{I_{chamber} + I_{duck}}{I_{chamber} + I_{duck} + I_{target}} \quad (1)$$

Not all of the backscattered electrons, however, were absorbed directly into the chamber and drawn up to the picoammeter. When high energy electrons enter a material such as the chamber wall, they can liberate electrons on the surface of the material. These secondary electrons have energies on the order of the work function of the material, around 50 V for steel. Despite their low energies, the secondaries often reach the target and skew the current measurements significantly.

In order to prevent secondaries from reaching the target, a low voltage potential wall was needed to deflect the secondaries back towards the chamber while having a negligible effect on the higher energy electrons that were being scattered off the target. This wall was provided by a cylindrical cage, known as the grid. 22 thin (50 μm) tungsten wires were wrapped around a copper frame that surrounded the target. The grid was placed on plastic blocks and positioned as to avoid contact with the target to ensure electric isolation.

Secondaries were also significant within the grid itself. Scattering off of the duckbill, for instance, was not negligible. To better understand secondaries within the grid, a positive bias was placed on the target and its effects studied in detail.

Data was taken with varying potentials, the grid bias ranging from -100 V to 0 V and the target bias from 0 V to 100 V. The variation of η under these changes was studied to gain insight into the behavior of the secondaries and to which applied voltages properly compensated for the effects.

Current Integration Systematics

The systematic uncertainties for the current integration mode are summarized in Table 1.

Table 1: Summary of the systematic uncertainties for the current integration mode

Effect	Uncertainty
Duckbill Correction	3%
Grid Secondaries	1%
Reproducibility	5%
Current Dependence	3%
Total	7%

To account for secondaries within the grid, a correction was devised which involved the solid angle subtended by the duckbill and the values of eta when the grid was not biased. The solid angle needed to correct the data and the true solid angle of the duckbill disagreed slightly, leading to a 3% systematic uncertainty.

Because the wires that comprised the grid were finite in size, they exposed a finite solid angle from which secondaries could be created. These secondaries could be accounted for at the 1% level.

Repeated experiments with varying bias and beam configurations showed the measurements of eta to be reproducible at the 5% level.

What few nonconducting surfaces were exposed produced some effects due to charging. Charging effects produced a current dependence in η at the 3% level.

These effects give a total fractional systematic uncertainty of 7% for eta in the current integration mode.

Silicon Detector Mode

In the silicon detector mode an angular distribution of the backscattering was measured. Energy spectra were taken at 20° to 80°, defined normal to the scintillator target (Fig 3), in increments of 10°. To test for the proper alignment of the target and detector, spectra were also taken for negative angles.

Typical beam currents used with the silicon detector were much smaller than those in the current integration mode. To minimize dead time in the data acquisition system, the beam currents were kept between 20 and 30 pA. For the electronic settings used, this current corresponded to a rate of about 20 kHz. The rate was carefully kept at or below 20 kHz in order to minimize pile up in the analog-to-digital converter.

Each raw spectrum is plotted as a function of digitized pulse height, proportional to energy deposited in the detector. On the vertical axis lies the number of counts, not corrected for any dead time in the data acquisition system. Dead time studies were performed with each measurement so that a dead time correction could be extrapolated and applied to each spectra.

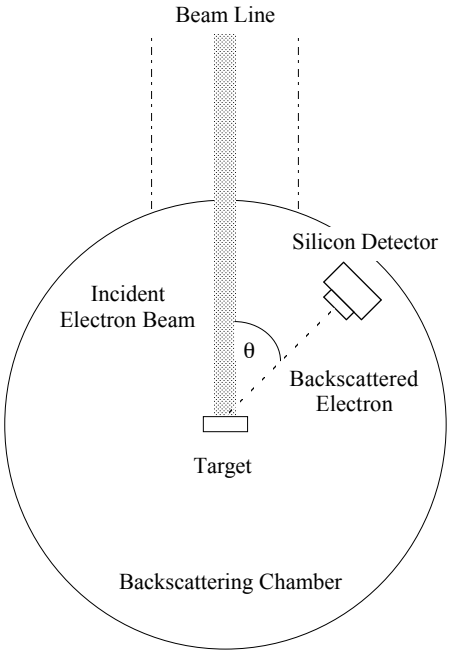

Figure 3: Schematic of the silicon detector configuration.

Since it is taken behind the target, the spectrum at 100° is free of any direct backscattering, and makes a reasonable background spectra for the rest of the data. This spectra will be subtracted from both the negative and positive angle data to obtain a background corrected data set. Previous studies have confirmed the validity of using the 100° spectra in this way, with associated systematic errors on the order of 3-5%.

Silicon Detector Systematics

Table 2 summarizes the fractional systematic uncertainties for the silicon detector measurements.

Repeated measurements with the silicon detector found that the data were reproducible to the 7% level. Previous studies found the true active area of the detector studies to have a systematic uncertainty of 4%. The solid angle effect of a finite beam spot area was known to be less than 5% $\sin\theta$. For the rates used, dead time corrections were reliable but pile up in the analog-digital converter required a 3% uncertainty.

Table 2: Summary of the systematic uncertainties for the silicon detector mode

Effect	Uncertainty
Reproducibility	7%
Active Area	4%
Finite Beam Spot	$5\% \times \sin\theta$
Dead Time	3%
Alignment	2%
Current Detection	3%
Damage	1%
Total	12% average

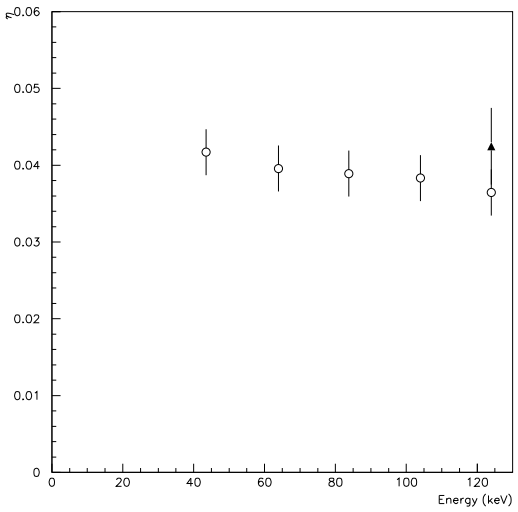

Figure 4: Final normal incident backscattering fraction for plastic scintillator. Empty circles show current integration data while the filled triangle shows the silicon detector result. The silicon detector data was larger than the current integration data, but both methods agree to the level of the systematic uncertainties.

While all efforts were made to ensure the proper alignment of the target, detector, and chamber, there was an uncertainty on the 0.5^o level. To quantify any misalignment in the apparatus, data was taken for both positive and negative θ. If the alignment was perfect these spectra would be equal save for statistical uncertainties. The residual systematic uncertainty for misalignment was taken to be 2%.

The Ortec current integrator used to measure the target current was calibrated against other picoammeters and was found to be accurate at the 0.3 pA level. Normalization of the data was then known to the 3% level.

Together these give, on average, a total systematic uncertainty of 12% for the silicon detector mode.

Results

Current Integration Mode

The final normal incident backscattering fractions for the current integration mode are plotted in Figure 4 with the result of the silicon detector data.

While studying the effect of beam current on eta, it was found that the large beam currents typically used for current integration studies were causing permanent damage to the plastic scintillator. If the beam current was any larger then ten nanoampheres, eta would slowly rise with time. This increase did not vanish if the beam current was reduced or even if the target was allowed to rest.

The increase did, however, vanish if the beam was moved to another position on the scintillator. Areas of the scintillator that had yet to be exposed to a high current beam would behave well until bombarded with high beam current. Visual observations showed a clear dimming of the beam as it passed through a depredated region, indicating a decrease in scintillating yield and damage within the scintillator.

Moreover these regions were clearly evident with the naked eye when the target was removed from the chamber. The scintillator was discolored, a brown tint indicating where the scintillator had been damaged by the beam.

This degradation of the scintillator was unknown and unaccounted for in previous studies. Beam currents used in previous studies were typically much higher than those found to be safe for these scintillator targets and may have resulted in uncontrolled and unaccounted systematic effects.

Silicon Detector Mode

The raw spectra measured by the silicon detector needed significant analysis before η could be extracted from the data. Once the background spectrum had been subtracted from each, the spectra were corrected for dead time then normalized by the incident beam current. At this point the channels were mapped to energies with an energy calibration that had been taken with the spectra. To facilitate further analysis, the data was plotted as a function of the dimensionless variable q, where $q = \mathrm{E}/\mathrm{E}_{beam}$.

These analyzed spectra for each angle are shown in Figure 5. For small angles, there is a pronounced peak around q=0.45. As the angle increases, the peak shifts towards higher q while flattening into a

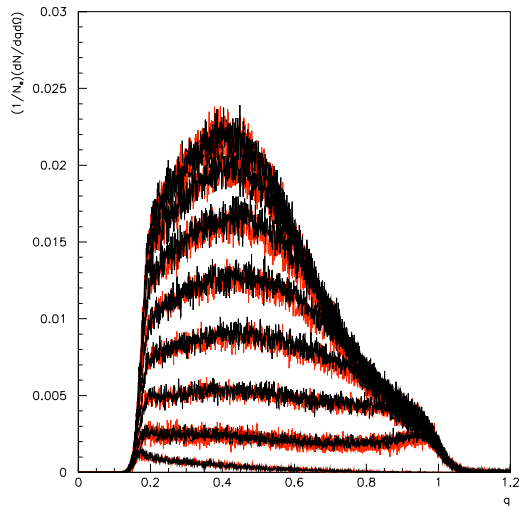

Figure 5: Normalized silicon detector specta of the normal incident backscattering fraction at E_{beam}=124 keV. The spectra are plotted as $1/N_e(dN/dqd\Omega)$ verses q. Assuming a perfect detector, the mantissa is $d\eta$ (dN/N_e) per unit q, per unit solid angle. Black spectra correspond to positive angles while the red specta correspond to negative angles. The smallest spectra is that of +/- 100°. Directly above this is the +/- 80° spectra, the spectra decreasing in increments of 10°. Largest of the spectra are those of +/- 20°.

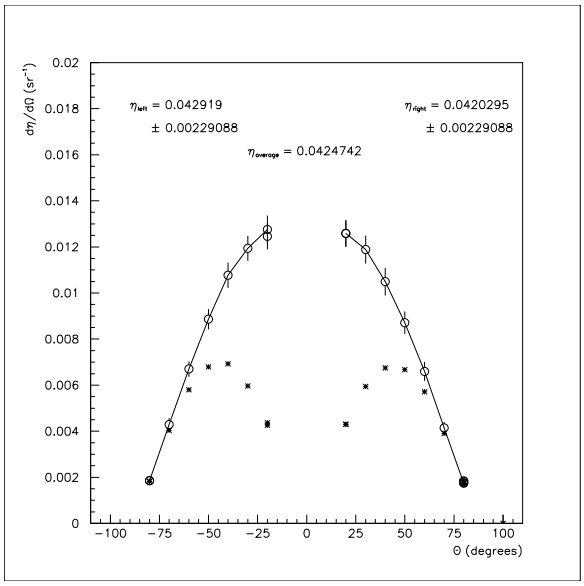

Figure 6: $\frac{d\eta}{d\Omega}$ (circles) and $\frac{d\eta}{d\Omega}\sin\theta$ (stars) as a function of θ. The numerical sum approximated the integral over θ well when compared to analytical models. To differentiate between those points included in the integral and those that were not, a line passes through all points used in the integration. The listed uncertainties are due only to the extrapolation. Systematic uncertainties were used in the final measurement.

level spectrum. This can be understood by considering the interactions between an incident electron and the target on a microscopic level. Interactions with the nuclei in the target deflect the path of the electron while interactions between the electrons of these atoms draw energy from the electron. Hence the more interactions between an incident electron and the nuclei, the longer the electron is in the target and the more energy it loses to the nuclear electrons. Most backscattered electrons scatter many times before deflecting out of the target at small theta. Though it is much rarer, electrons may also scatter only a few times, leaving the target with more energy and at larger θ. This explains the shifting and dissipation of the peak rather well. As the angle increases, electrons that reach the detector must scatter less, hence they are left with more energy to deposit and a peak at higher q. Fewer scatters, however, are increasingly less probable, so at these higher angles the peak must decrease, as seen in the spectra.

Since the data is to be compared to the current integration measurements, the spectra must be integrating over q and solid angle. The integration over q is easily performed at high q by numerically summing the counts in each bin. At low q, however, the spectra is dominated by noise in the detector and the data acquisition system which leaves little information regarding the true spectrum. To correct for this, all data below q=0.2 were removed from the spectra and linear fits were made from the from the remaining data at small q to extrapolate the spectra down to q=0. This extrapolation was then summed with the remaining spectra to obtain the necessary integrals.

The numerical integrations gave $\frac{d\eta}{d\Omega}$ as a function of θ. η is then

$$\eta = \int_\Omega \frac{d\eta}{d\Omega} d\Omega \tag{2}$$

$$\eta = \int_0^{2\pi}\int_0^{\pi/2} \frac{d\eta}{d\Omega}\sin\theta d\theta d\phi \tag{3}$$

Or assuming η to be independent of the azimuthal angle ϕ,

$$\eta = 2\pi\int_0^{\pi/2} \frac{d\eta}{d\Omega}(\theta)\sin\theta d\theta \tag{4}$$

Each $\frac{d\eta}{d\Omega}$ were then multiplied by sin theta before being summed to give a numerical approximation to

the integral. Both $\frac{d\eta}{d\Omega}$ and $\frac{d\eta}{d\Omega} sin\theta$ are shown in Figure 6.

The result of the integrations is a final value of η from the silicon detector data. Values of η obtained from the current integration mode and the silicon detector mode are plotted in Figure 4. While the measurements obtained with the current integration mode are smaller than those obtained with the silicon detector mode, the difference is within the systematic uncertainties signifying good agreement between the two methods.

Conclusion

Detailed studies of the normal incident backscattered fraction for polyvinyltoluene plastic scintillator at energies in the range of neutron beta decay were performed. Two methods were compared and were found to agreed to the level of systematic errors. Both studies specifically addressed the problems that were though to have caused uncontrollable systematic uncertainties in previous studies, namely the quality of the scintillator used and the effects of charging in the scintillator. The new, aluminized plastic scintillators performed well, and the data was dominated by any systematic uncertainty that was relatively well understood. Moreover, a previously unknown systematic uncertainty was discovered during this study. Damage of the scintillator due to large beam currents was found to have a significant effect on the normal incident backscattered fraction. Appropriate measures were taken to account for the damage and account for the systematic uncertainty. The data collected in this study will be used to calibrate Monte Carlo electron transport simulations. These properly calibrated simulations will be used to correct for backscattering effects in the approaching UCN-A experiment, producing the precision demanded by the parameters of the experiment.

References

[1] P. Gérard *et al.*, Scanning **17**, 377 (1995)

[2] G. R. Massoumi *et al.*, Phys. Rev. Lett **68**, 3873 (1992)

[3] G. R. Massoumi *et al.*, Phys. Rev. B **47**, 11 007 (1993)

[4] S. Agostinelli *et al.*, GEANT4 Collaboration, Nucl. Instrum. Methods Phys. Res. A **506**, 250 (2003)

[5] T. Bowles and A. R. Young (co-principal investigators), a proposal for an accurate measurement of the neutron spin, electron angular correlation in polarized neutron beta-decay with ultracold neutrons, 2000.

[6] J. Yuan *et al.*, Nucl. Instrum. Methods Phys. Res. A **465**, 404 (2001).

[7] J. W. Martin, *et al.*, Phys. Rev. C **68**, 055503 (2003).

Acknowledgements I would like to thank my mentor, Jeff Martin, for his generous contribution of knowledge, time, and effort. Also, I would like to express my gratitude to everyone in Kellogg 00 for all their help. This work was supported by the Caltech Summer Undergraduate Research Fellowship program.